# Characterization of Postsynaptic Glutamate Transporter Functionality in the Zebrafish Retinal First Synapse Across Different Wavelengths

**Marco Garbelli[1], Stephanie Niklaus[1] & Stephan C.F. Neuhauss[1,§]**

[1]University of Zurich, Department of Molecular Life Sciences, Winterthurerstrasse 190, CH-8057 Zurich, Switzerland

[§] Corresponding author:

Prof. Dr. Stephan C. F. Neuhauss
Department of Molecular Life Sciences
University of Zurich
Winterthurerstrasse 190
CH-8057 Zurich, Switzerland
stephan.neuhauss@mls.uzh.ch

## Abstract

In the zebrafish retina, incident light undergoes wavelength-dependent processing encompassing mechanisms such as color opponency, contrast enhancement, and motion detection prior to neural transmission to the brain proper. In darkness, photoreceptors continuously release glutamate into the synaptic cleft, a process that diminishes in response to increased light intensity, thereby conveying visual signals to ON and OFF bipolar cells. Specifically, in zebrafish, the ON pathway signal transduction is mediated by metabotropic glutamate receptor 6b (mGluR6b) and Excitatory Amino Acid Transporters (EAATs). Here we demonstrate that knockout of *eaat5b* and *eaat7* disrupts electroretinogram responses to short and long-wavelength stimuli while preserving middle-wavelength responses, suggesting wavelength-specific roles. We found differential expression of EAAT5b and EAAT7 in the outer plexiform layer, particularly in the strike zone, crucial for prey capture, supporting task specific involvement of these signaling pathways. In order to investigate this, we developed a virtual hunting assay using UV light stimuli. Such a behavioral assay targeting short and long wavelengths indicate that EAAT5b and EAAT7 influence UV-dependent prey detection and motion sensing differently. Our findings highlight the importance of EAAT5b and EAAT7 in modulating light integration dynamics in the zebrafish retina.

## Introduction

The developing zebrafish retina represents an exquisite example of functional adaptation and optimization to the visual environment these fish inhabit. Zebrafish are found in the Indian subcontinent, living in shallow ponds and still water bodies such as rice fields (Spence et al., 2008). During monsoon season they can be found in streams and rivers with a low flow regime where these animals mostly occupy its margins (Spence et al., 2008). Being diurnal animals with a cone-dominant retina, the adult photoreceptor layer features a uniform mosaic structure where the different photoreceptor subtypes are homogeneously distributed over the whole surface (Allison et al., 2010). In the wild, zebrafish larvae are exposed to the full spectrum of sunlight passing through the shallow waters in which they reside. Compared to the crystalline organization found in the adult photoreceptor layer, the larval eye displays marked anisotropies in the distribution of cell types in both outer and inner retina, possibly to capitalize on the environmental lightning (Zimmermann et al., 2018). Photoreceptor subtypes and their

underlying chromatic and achromatic networks present higher densities in specific regions that match with the distributions of wavelengths found in its natural environment (Zimmermann et al., 2018). Dissection of the zebrafish visual circuits organization revealed the existence of at least three non-opponent achromatic axes (achromatic-OFF, UV-ON, Red ON-OFF) and an equivalent number of opponent chromatic ones (UV/RGB, R/G, RG/B) (Orger and Baier, 2005; Zimmermann et al., 2018; Yoshimatsu et al., 2020; Bartel et al., 2021). Amongst the achromatic ones, the UV-ON and the Red ON-OFF axes appear to be directly involved (if not essential) in specific behaviors such as prey-capture for the former (Yoshimatsu et al., 2020) and motion sensing for the latter (Orger and Baier, 2005). This suggests that the structure of the larval retina is adapted to maximize the extraction of environmental information, thereby enhancing the accuracy and sensitivity of behaviors essential for vital functions such as feeding and navigation. However, the internal processing within the central nervous system that regulates these circuits remains less understood. In zebrafish larvae, the majority of visual pathways are established at the first synapse (Yoshimatsu et al., 2021). Here, the wavelength components of incoming light are separated by the four cone subtypes. Distinct horizontal cells (HCs) groups subsequently contribute to the generation of the first opponent axes (R/G, RG/B) (Yoshimatsu et al., 2021). Bipolar cells (BCs) receive these signals and transmit it to ganglion cells (GCs) with further modulation from amacrine cells (ACs). Finally, GCs will send the processed information directly to the brain proper. It was recently demonstrated that the inner retina is crucial for establishing two of the known visual axes (achromatic-OFF, UV/RGB) and for the introduction of a temporal component to the response (transient or sustained) (Bartel et al., 2021; Wang et al., 2023). However, most of the chromatic processing is computed at the first retinal synapse and is conserved throughout the vertical pathway. In darkness, photoreceptors are depolarized and tonically release glutamate in the synaptic cleft. This causes OFF-bipolar cells that express glutamate ionotropic receptors to depolarize upon light decrease (Euler et al., 2014). Conversely, ON-bipolar cells express a metabotropic glutamate receptor (mGluR6), which causes the blocking of TRPM1, a constitutively open cation channel (Morgans et al., 2009; Morgans et al., 2010). When light strikes the eye, the photoreceptors hyperpolarize and gradually reduce glutamate release. This leads to a reopening of TRPM1 and depolarization of the ON bipolar cell (Morgans et al., 2009). Electrophysiological experiments confirmed that in zebrafish ON-bipolar cells a second mechanism regulates depolarization (Wong and Dowling, 2005). This is mediated by a group of postsynaptic glutamate transporters from the Solute Carrier (SLC1) family (Niklaus et al., 2024). These transporters act as dual-purpose proteins, carrying glutamate, three Na+ and one H+ inside the cell and counter-transporting K+ (Fahlke et al., 2016), consequentially generating a thermodynamically uncoupled current by Cl- flow (Fairman et al., 1995; Mim et al., 2005), able to control ON-response to light along with the human homolog mGluR6b. Zebrafish *eaats* complement features 11 members distributed at different locations in the central nervous system (Gesemann et al., 2010; Niklaus et al., 2017). Of these, only EAAT5b and EAAT7 are located in the dendritic tips contacting the majority of photoreceptors (Niklaus et al., 2024). Electroretinogram experiments on *eaat5b*$^{-/-}$, *eaat7*$^{-/-}$ and double mutant larvae exposed to wide field white light show that the two transporters impact differentially ON-BCs depolarization in both amplitude and dynamics. Namely, lack of EAAT5b causes a modest lowering of the max

amplitude and a steep reduction of the time-to-peak of the wave, while loss of *eaat7* does not lead to an amplitude effect and makes the ON-BCs depolarize slower (Niklaus et al., 2024). Previous studies indicate that mGluR6b-dependent ON-response might have a wavelength-dependent tuning (Saszik et al., 2002; Nelson and Singla, 2009). By performing monochromatic ERG (Zang et al., 2015), we observed that lack of either EAAT5b or EAAT7 leads to moderate defects in the ON-response only under certain wavelength ranges. Interestingly, lack of either Eaat5b or Eaat7 leads to long-wavelength response defects only. Conversely, when both factors are absent, the defect becomes observable for short-wavelengths responses as well. Analysis of the distribution of these transporters through the whole larval outer plexiform layer (OPL) revealed a complementary pattern for the two postsynaptic Eaats, where EAAT5b appears to concentrate in the "area temporalis" or "strike zone" (SZ), an important region for prey detection and capture (Zimmermann et al., 2018; Yoshimatsu et al., 2020). We developed a behavioral assay based on UV-light stimulation to evaluate the hunting response in our mutants and found no significant differences in *eaat5b* mutants. However, *eaat7* mutants displayed a significant increase in responses to our stimulation, suggesting a role of these genes in regulating UV-signal integration for prey capture. Optomotor response (OMR) analysis targeting red cones demonstrated a defect in motion detection in eaat5b-/- larvae, whereas eaat7-/- mutants exhibited no detectable defects. These findings suggest that EAAT5b and EAAT7 regulate distinct aspects of ON signal transmission dynamics at the level of bipolar cells (BCs), with mGluR6b acting as the primary regulator of response amplitude.

## Results

### EAAT5b and EAAT7 present spectral-specific inputs to the ON-response

Previous publications studying the spectral characteristic of ON-response regulation suggested that both metabotropic and non-metabotropic components of this machinery might possess wavelength-specific responses (Saszik et al., 2002; Nelson and Singla, 2009). To assess whether Eaat5b and Eaat7 show any chromatic tuning, we tested mutants in these two *eaat* genes with color-channel-specific ERG recordings (Zang et al., 2015; Niklaus et al., 2024). Interestingly, neither UV-blue nor green light stimulation led to any significant effect on the b-wave amplitude (proxy of ON-BCs depolarization) between both *eaat5b* and *eaat7* KO animals when compared to WT (Figure 1A- B; 1D-E). Red light stimulation however, caused a decreased b-wave amplitude throughout all 5 log units in both *eaat5b*$^{-/-}$ (adjusted p-values of 0.0331, 0.0127, 0.0331, 0.0331, 0.0009 respectively) and *eaat7*$^{-/-}$ (adjusted p-values of 0.037, 0.013, 0.011, 0.005, 0.006 respectively) larvae (Figure 1C-F). Monochromatic ERG recordings on double *eaat5b*$^{-/-}$; *eaat7*$^{-/-}$ mutant fish displayed a decreased b-wave amplitude both when stimulated with UV-blue (log-3: 0.024 adjusted p-value, log-2: 0.022 adjusted p-value, log-1: 0.022 adjusted p-value) as well as red (log-2: 0.023 adjusted p-value) light (Figure 1G-I). This suggests that neither EAAT5b nor EAAT7 participate in green light signal transmission, but one of these transporters might be involved in transmitting short-wavelength light information, originating from either blue or UV cones.

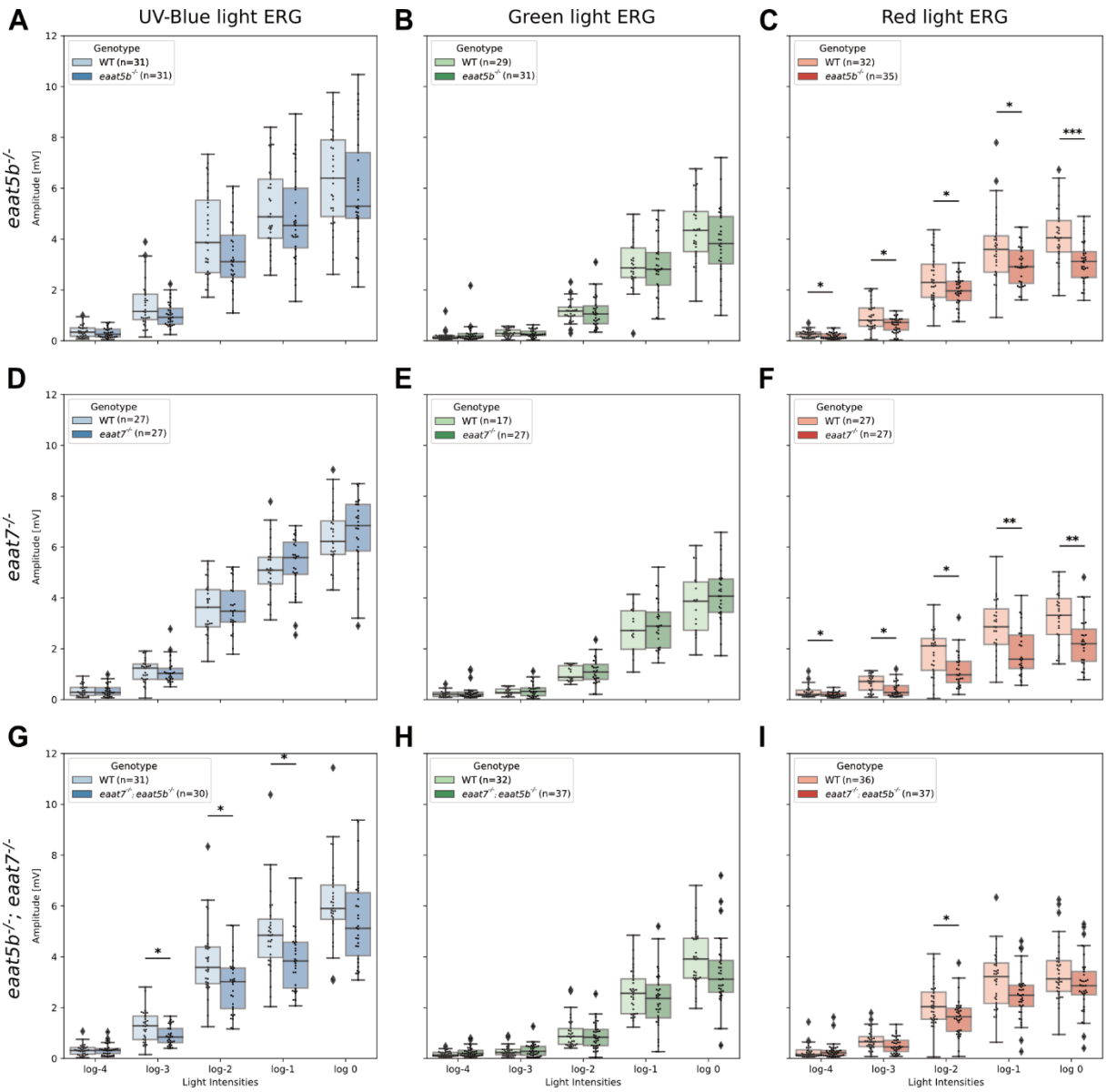


**Figure 1: EAAT5b and EAAT7 mediate UV-blue and red but not green light signal transmission.**
Monochromatic ERG was recorded on *eaat5b*$^{-/-}$ (A-C), *eaat7*$^{-/-}$ (D-F) and *eaat5b*$^{-/-}$*; eaat7*$^{-/-}$ (G-I). B-wave amplitudes are plotted in box-and-whisker plots with fish-specific data overlaid as a swarmplot. Homozygous mutation in *eaat5b* or in *eaat7* causes a decrease in the b-wave if stimulated red light (C and F) but not if stimulated with green or UV-blue light (A, B, D and E). Double KO animals display a reduced b-wave amplitude for UV-blue (G) and red light (I) but not for green light (H).

## Distribution of Eaat5b and Eaat7 partially reflects cones anisotropies

We set out to examine the expression patterns and locations of these two proteins across the outer plexiform layer in order to explore the mechanisms behind these wavelength-specific responses. In a previous study, we have shown that EAAT5b and EAAT7 co-localize at the dendritic terminal of bipolar cells in contact with all the cone types and with some rods in the adult retina (Niklaus et al., 2024). While the zebrafish adult photoreceptor cell layer displays a rather homogeneous mosaic structure (Allison et al., 2010), the larval eye features strong anisotropies in the distribution of the different cone types (Zimmermann et al., 2018). In particular, UV cones are strongly enriched in the “strike zone” (SZ), a temporo-

ventral region of the retina where this photoreceptor subtype displays morphological and functional changes resulting in higher sensitivity and slower signal integration dynamics (Zimmermann et al., 2018; Yoshimatsu et al., 2020). We performed whole mount immunohistochemistry on 6 dpf dissected retinas, imaging most of the outer plexiform layer (OPL) and recording EAAT5b, EAAT7 and both UV and red cone pedicles in order to document any EAAT5b and EAAT7 and to test if these transporters' distribution is biased towards a single or more cone types. Maximum projections of WT retinas show that these two proteins appear to co-localize along the whole retina (Fig. 2A) as previously observed (Niklaus et al., 2024). However, the relative intensity of each transporter changes in different regions of the OPL, with EAAT7 intensity dropping in the temporal area of the eye, where instead EAAT5b signal increases (Fig. 2A dashed line). To further investigate this uneven distribution, we selected virtual midsections (see methods) from the recorded eyes and calculated the relative intensities of EAAT5b, EAAT7 and UV/red cone pedicles respectively, starting each measurement from the ventral part of the SZ (Fig. 2B). Virtual midsections show that EAAT5b signal reaches peak intensity in the SZ, while EAAT7 shows the highest signal in the nasal patch of the retina. As observed by the UV cones staining and previously published work (Yoshimatsu et al., 2020), UV cone pedicles are concentrated exactly in the peak intensity regions of both EAAT5b and EAAT7 (Fig. 2C). Relative intensity plots, pooling the whole set of recorded retinas (n = 11), confirm what was already observed from the microscope images, further highlighting the similarities in the EAAT5b and UV cones recorded traces and pointing out the markedly higher intensity of EAAT7 in the nasal region of the retina (Fig. 2D top panel). A correlation matrix of all the traces shows that UV cones strongly correlate with EAAT5b, while EAAT7 shows lower similarities (Fig. 2D bottom panel). We successively investigated the retinas from the red cones reporter line (Fig. 2E). These photoreceptors mostly populate the dorsal half of the retina, becoming scarcer close to the SZ (Fig. 2E). EAAT5b and EAAT7 traces showed similar intensity patterns to what was observed in the previous experiment, but neither of the two proteins distribution fitted the intensity profile of the cone pedicles as previously seen for UV cones and EAAT5b (Fig. 2F Top). However, the correlation matrix indicates high similarity between EAAT7 and red cone pedicles (Fig. 2F bottom panel). The discovery of the existing anisotropy between EAAT5b and EAAT7 led us to inquire on mGluR6b distribution in the OPL. Preliminary data (N=1) shows that the metabotropic receptor's distribution along the retina follows a similar, if even narrower, pattern as the one shown by EAAT5b (Fig. S1). We know from previous publications that the use of an mGluR6b agonist drug can lead to monochromatic ERG defects that are stronger for short wavelength stimulation compared to the rest of the spectrum (Saszik et al., 2002). It is possible that this defect would stem from a higher concentration of mGluR6b in the dendritic terminals contacting UV cones consequently more affected by the block. Taken together, these results suggest that EAAT5b and EAAT7 have different functions in the larval anisotropic retina. Even if both localize in contact with UV and red cones, our data suggest a difference in expression ratio between the two, indicating subspecialized role in the different retinal compartments. UV cones in the SZ are crucially important for successful prey detection. Previous studies hypothesize that UV cones residing in the nasal patch are relevant for predator avoidance (Yoshimatsu et al., 2020). This suggests that the different biophysical properties previously observed in EAAT5b and EAAT7 (Niklaus et al., 2024) might aid the information acquisition for one or the other behavior.

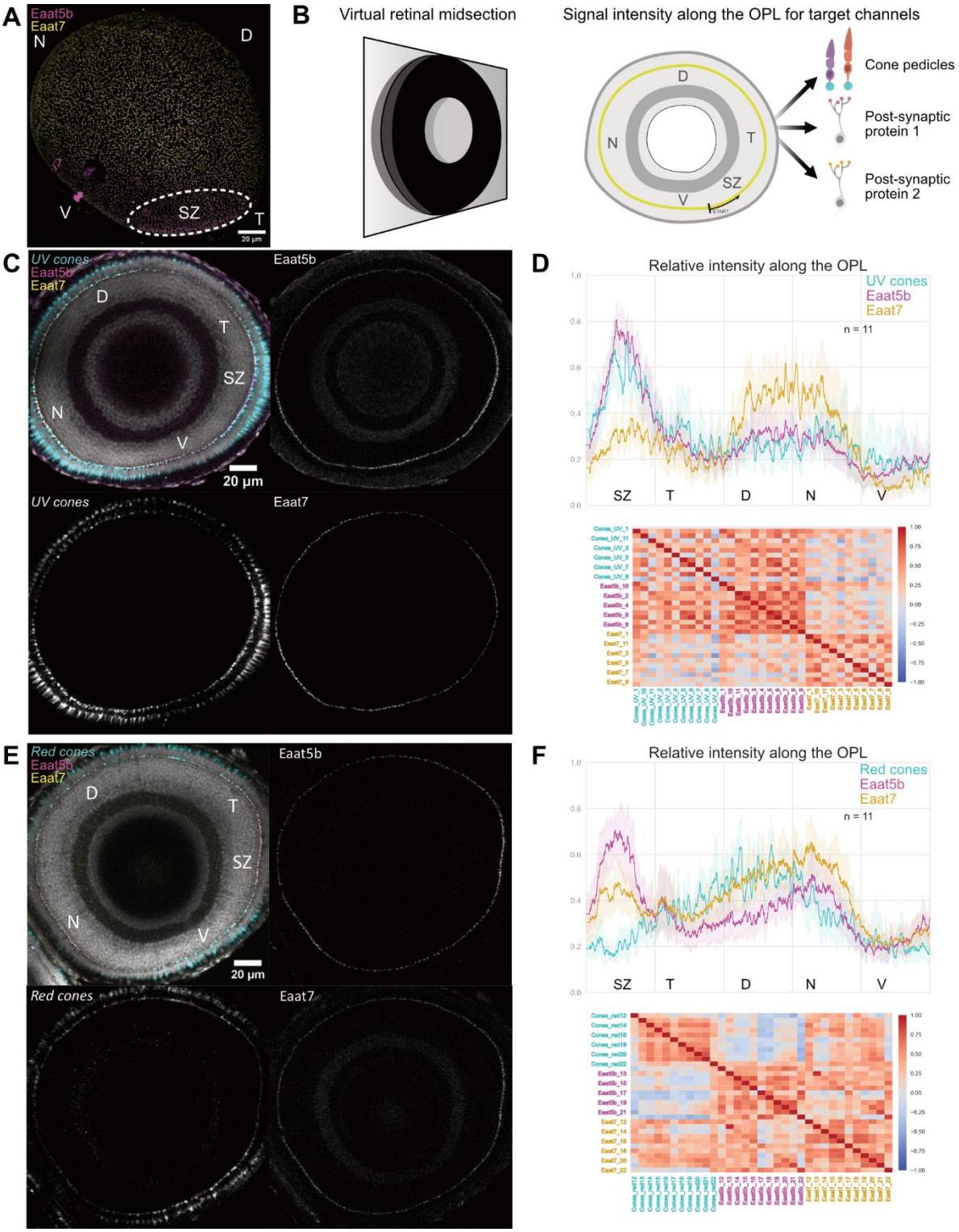


**Figure 2: EAAT5b distributes anisotropically to EAAT7 and focuses in the Strike Zone in contact with UV cones.** (A) Projection of the 6 dpf whole larval retina stained for EAAT5b (magenta) and EAAT7 (yellow) shows that both proteins appear co-expressed along most of the OPL apart from the temporo-ventral area called SZ where relative intensity of EAAT7 drops while EAAT5b raises, indicating distribution anisotropy. (B) Schematics depicting the process used to measure the relative intensity of fluorescent signals along the OPL. Left: One section (retinal midsection) where most of the photoreceptor layer is perpendicular to the z-axis is selected. Right: on the selected section, the signal intensity for the different channel is measured by tracing a line along the visible OPL starting from the ventral extreme of the SZ and the average grey level under the trace is recorded and normalized to have values between zero and one for all channels. (C) Virtual midsection of a 6 dpf WT retina with nuclei

(grey), UV cones (cyan), EAAT5b (magenta) and EAAT7 (yellow) labelled. (D) Top: Relative intensity values of the three fluorescent channels along the whole OPL. Full-colored line represents the traces' mean and semitransparent area represents 95% CI. Bottom: Pearson's correlation matrix pooling all the measured traces. While the overall correlation score is relatively high, probably due to partial co-localization, EAAT5b and UV cone pedicles appear to define a cluster on their own when compared to Eaat7 traces. (E) Virtual midsection of a 6 dpf WT retina with nuclei (grey), Red cones (cyan), EAAT5b (magenta) and EAAT7 (yellow) labelled. (F) Top: Relative intensity values of the three fluorescent channels along the whole OPL. Full-colored line represents the traces' mean and semitransparent area represents 95% CI. Bottom: Pearson's correlation matrix pooling all the measured traces. Notably, while EAAT7 and EAAT5b still correlate with a high score amongst each other, the former's traces appear to be more similar to red cone pedicles compared to EAAT5b. This is probably due to the differences at the Strike Zone. For the whole panel, "N": nasal, "D": dorsal, "T": temporal, "V": ventral, "SZ": strike zone.

## Zebrafish display hunting response in an intensity-dependent trend

Both zebrafish short wavelengths cones (UV and blue) have mostly overlapping wavelength-detection ranges (Yoshimatsu et al., 2021). This makes isolation between these two cone populations using a wide field stimulus non-trivial. Larval hunting strongly relies on the specialized UV cones residing in the SZ and their ablation drastically impairs prey detection as seen in published behavioral assays (Yoshimatsu et al., 2020). Our previous results point towards EAAT5b having a role in UV signals integration and its peculiar concentration in the SZ might be explained by a function in prey detection signaling. Testing differences in sensitivity with this innate larval behavior could help differentiate between a functional defect stemming from either UV or blue cones. Therefore, we built a behavioral setup to evoke a hunting response in zebrafish larvae using an artificial and programmable UV stimulus. The setup records the behavior of a single larva head-mounted in an arena with a screen where a single UV dot is projected from a focused LED source (Fig.3A). The UV LED is inserted in a scaffold holding lenses and a pinhole that focuses the light in a single small dot roughly the size of a paramecium (~4.9°) (Fig. 3B). A servomotor at the base of the LED scaffold provides movement to the stimulus and both movement and LED control are defined by a computer-triggered Arduino (Fig. 3C). Eye convergence and tail flick events can be then recorded and identified as hunting events (Fig. 3D). Virtual hunting assays have been previously used to have a higher control over stimulation through the use of projectors displaying white dots on a darker background (Bianco et al., 2011; Semmelhack et al., 2014). Due to the nuances of our setup, we decided to validate it by exposing WT larvae to max intensity stimuli with LEDs that would target shorter and longer wavelength cones respectively (Fig. 3E). 6 dpf WT larvae were exposed to ten rounds of stimulation at max intensity, consisting of a leftward and rightward stimulus in succession. The same larva was exposed first to orange light and successively to UV, following the same stimulation pattern. As expected, zebrafish larvae strongly react to a virtual hunting stimulus in the UV wavelength range (Fig. 4B), but have very limited response to light targeting the middle-/long-wavelength cones (Fig. 4A). Interestingly larvae showed an initial higher response, waning off by the 10$^{th}$ repetition, probably due to stimulus habituation. We next tested if the UV stimulus detection was intensity-dependent and if a "detection threshold" could be identified. For this, we exposed WT 6 dpf larvae to an increasing intensity paradigm, where the 10 rounds would expose the zebrafish to a range of intensities starting from 0% to 90% (Fig. 4B). Following our expectation, the number of

recorded hunting responses steadily increased along with the stimulus strength from intensity 40%, reaching a plateau around intensity 70%. In sum, we successfully built a behavioral setup that can stimulate zebrafish larvae with a programmable UV prey-like stimulus. We validated the machine following a similar paradigm already done with live prey (Yoshimatsu et al., 2020) and observed that larvae strongly react to UV light compared to orange. Moreover, we could demonstrate that number of responses is dependent on the stimulus intensity and that with our setup WT larvae can generally detect the stimulus starting from 40% of intensity. This suggests that this setup can be used to test UV sensitivity in our mutant larvae.

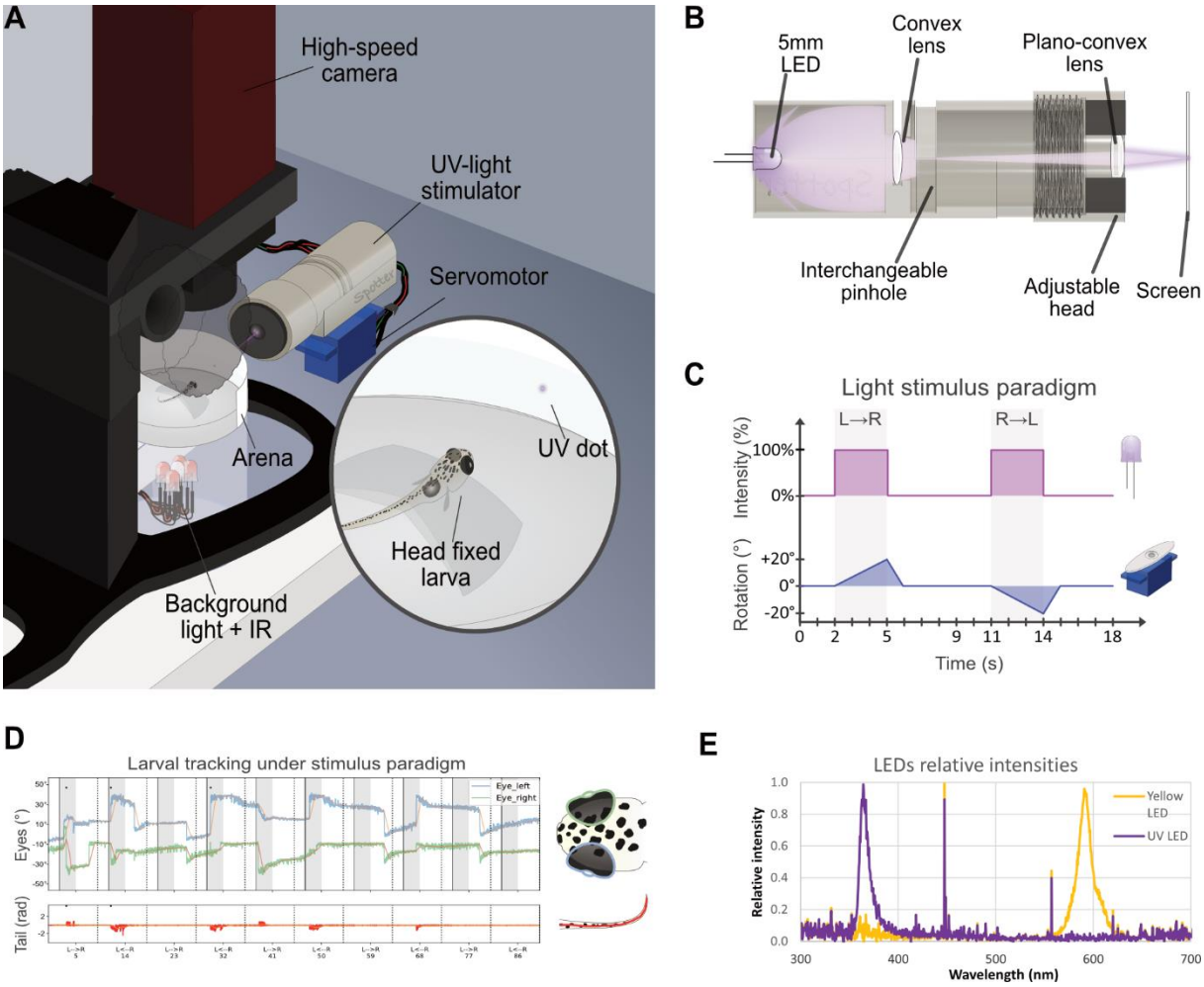


**Figure 3: UV stimuli can be used to simulate UV-bright moving paramecia in a LED-based custom setup.**
(A) Schematics of the custom setup used to deliver virtual prey-capture stimuli. (B) Schematics representing a section of the UV-light stimulator and approximate light pathway through pinholes and lenses. (C) Diagram representing the stimulus paradigm during one iteration. After two seconds from the start of the round, the LED turns ON along with the servomotor, which turns left to right by 20° (~90° on the projected screen). This takes three seconds, after which the LED turns OFF and the servomotor resets position. The same operation reiterates in the opposite direction after four seconds. (D) Sample tracking graphs from the setup. Top panel represents eye-specific angle variations over time (blue and green) with rolling averages used to identify events in orange. The bottom panel represents tail total curvature over time (red) with rolling average used to identify events in orange. Dots represent a detected event. (E) Relative intensities of the UV and yellow LEDs used for the validation measured by spectrometer.

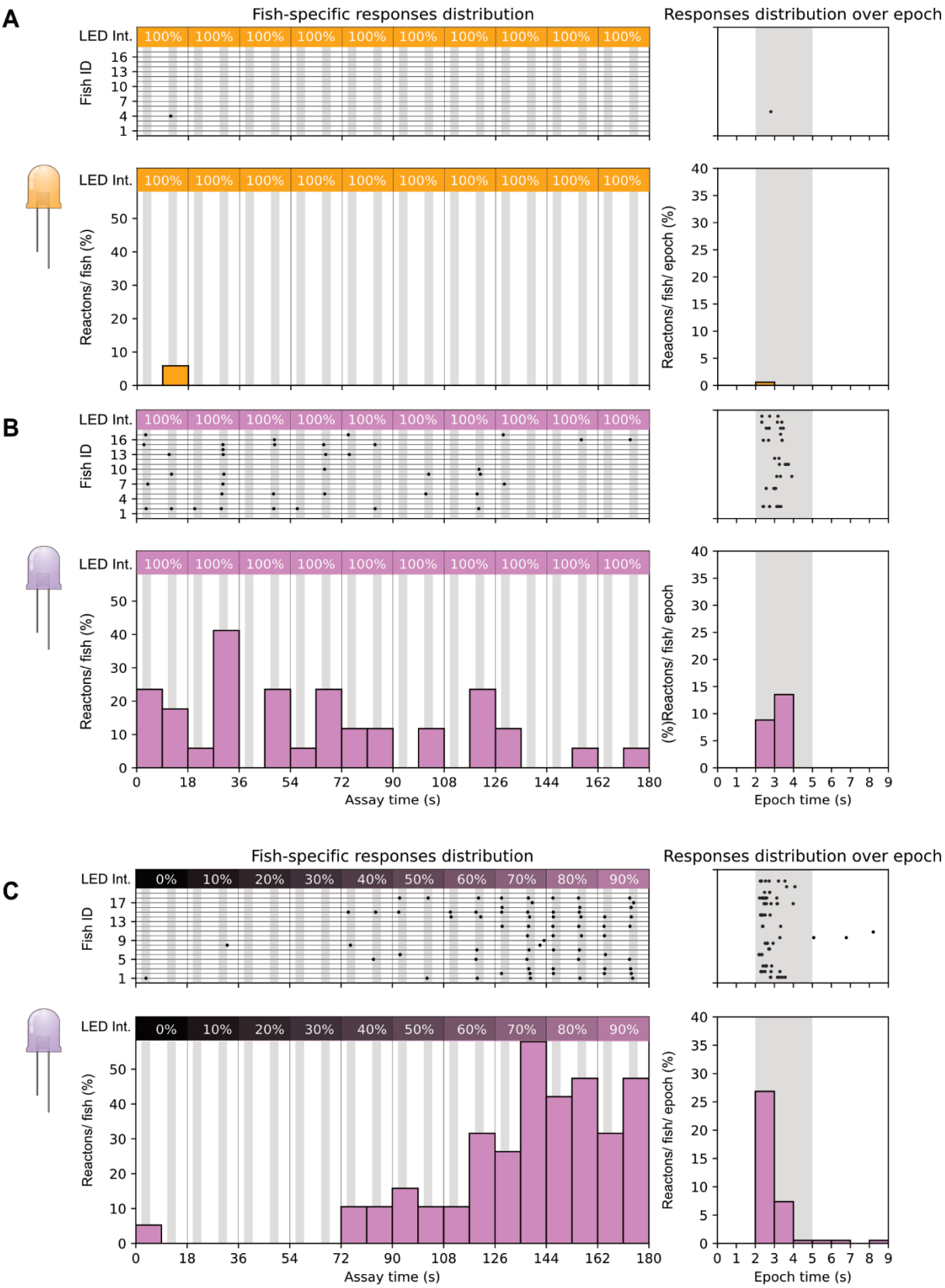


**Figure 4: Larval zebrafish show hunting response preferentially to UV stimuli in an intensity-dependent trend.** 6 dpf WT zebrafish larvae were exposed to yellow (A) and UV (B) full intensity hunting stimuli. While response was extremely low for the yellow light (1 response overall; A), UV stimuli elicited consistent response in the firsts stimulation rounds, gradually waning through each repetition (B). WT larvae exposed with incremental UV light intensity showed increasing response rates, reaching a response plateau between the last two intensity levels

(C). For all graphs in the figure: top shows fish specific results through the whole assay (left) and pooled events distribution over single epoch (right); bottom shows summary statistics as response percentages (reactions/fish on the left, reaction/fish/epoch on the right).

## Loss of EAAT7 positively affects prey detection sensitivity

Whole mount retina imaging shows that both EAAT5b and EAAT7 are expressed at the dendritic tips of UV cones, being concentrated in the SZ and in the nasal patch respectively. Monochromatic ERG recordings show that KO of both *eaat5b* and *eaat7* leads to a reduced b-wave in larvae stimulated with short wavelength light. Both protein localization (the SZ is an essential region for prey-capture (Zimmermann et al., 2018; Yoshimatsu et al., 2020)) and functional data point towards EAAT5b being involved in UV vision and prey detection. To prove this, we tested *eaat5b*$^{-/-}$ mutant larvae with the UV hunting sensitivity assay we previously validated. 6 dpf WT fish (n=25) and *eaat5b*$^{-/-}$ mutants (n=23) were exposed to our UV incremental intensity hunting assay (see methods). The animals were tested in alternate order to avoid potential circadian differences and the results were obtained from four different experimental days. Our experiments show that even if scarcely (4%), WT larvae can react to the UV stimulus already with 30% of LED intensity (Fig. 5A), while mutants lacking EAAT5b start responding from intensity at 40% (Fig. 5B). While response peak is reached in both genotypes at 80% intensity, WT larvae have a stimulus detections success of 44% (Fig. 5A), *eaat5b*$^{-/-}$ mutants show a lower response (35%) (Fig. 5B). However, neither the comparison of the proportion between successful hunting responses over total stimuli through the whole test, nor the one between responses distributions across the intensity levels resulted in a significant difference (two proportions z-test p-value: 0.16; Kolmogorov-Smirnov test p-value: 0.83) (Fig. 5C). This indicates that either our assay is not sensitive enough to detect a diminished UV-prey-detection defect indeed there is no such defect in *eaat5b* mutants. We then proceeded by testing *eaat7* mutants using the same paradigm. Interestingly, *eaat7* mutants (n=19) displayed overall better responses when compared to the WT larvae (n=18) (Fig. 6 right panel). While the latter could still detect the stimulus from intensity 30% (~5%) (Fig. 6A left), *eaat7*$^{-/-}$ fish started reacting to UV from intensity 20% (~5%) (Fig. 6B left panel). Response peak is reached at 60% for the controls and between 80 and 90% for the mutants; with WT larvae with a response of 33% while *eaat7* mutants reach 53% of response (Fig. 6 left panel). By comparing pooled responses over the total of delivered stimuli, we discovered that WT animal performed less than *eaat7* mutants did (two proportions z-test p-value: 0.0011; Fig. 6C left panel). Conversely, the comparison intensity-specific responses distributions led to no significant difference (Kolmogorov-Smirnov test p-value: 0.17) (Fig. 6C right panel). Taken together, our assay shows that lack or presence of both the postsynaptic EAATs might impact response to UV light and prey capture and, interestingly, the lack of EAAT7 appears to facilitate prey detection. Previous studies from our group (Niklaus et al., 2024) show that EAAT5b and EAAT7 have different gating dynamics along with different chloride current generation capacity. Hence it is conceivable that the lack of one or the other factor changes signal responses and information integration in important areas such as the SZ, thus altering the larva ability to detect and respond to a prey stimulus.

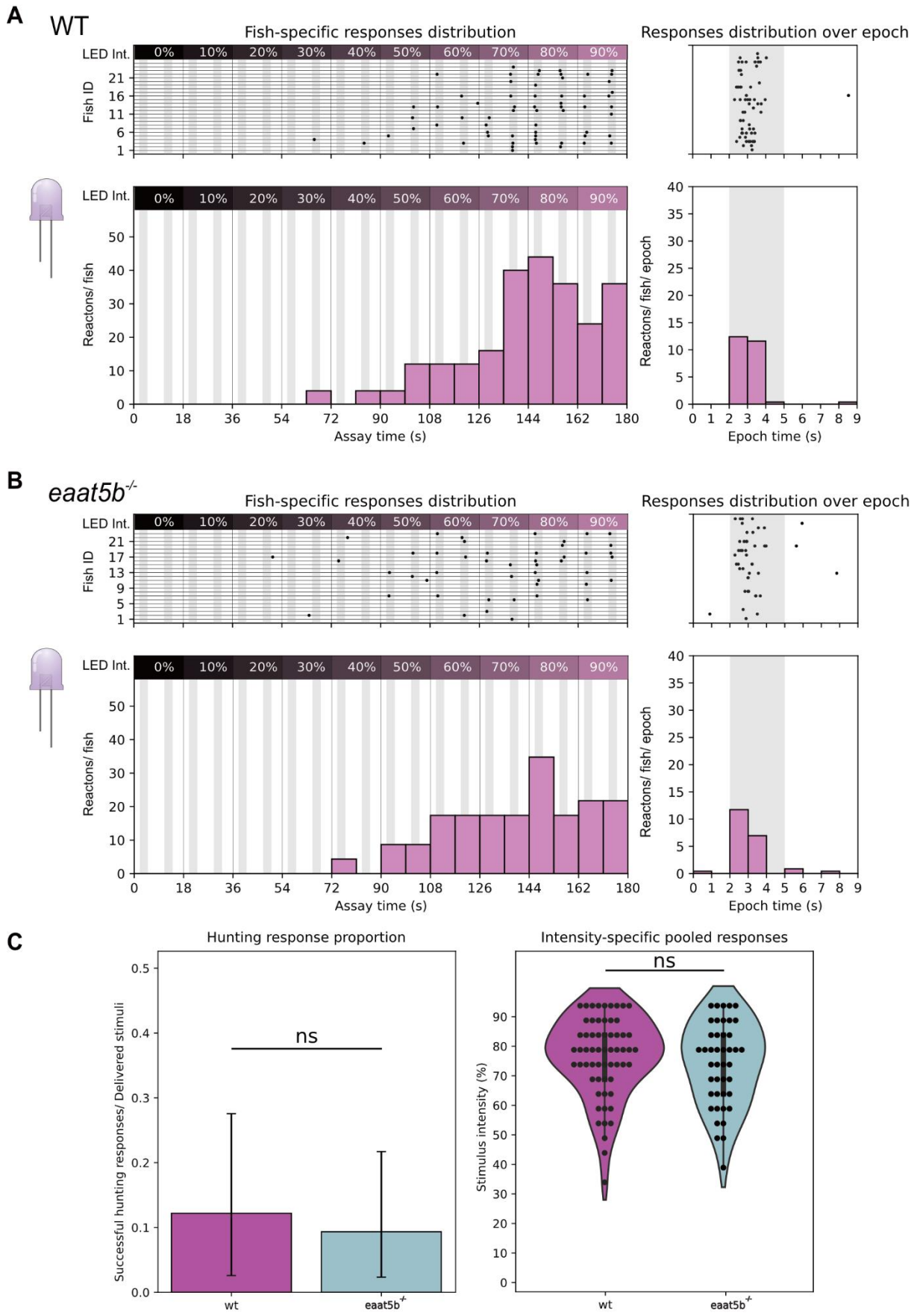


**Figure 5: *eaat5b* KO mutants do not show a significant difference in UV hunting response compared to WT.**

*eaat5b* mutants (n=23) begin reacting to the incremental prey stimulus one intensity-step later than WT (n=25) and display overall lower reactions/fish. While WT larvae start showing responses with stimuli delivered already at 30% of intensity (A), *eaat5b* mutants start showing reactions from 40% (B left). WT larvae reach peak responses at intensity 80% with a markedly higher response (A) compared to *eaat5b* mutants (B). Pooled responses proportion does not show any significant difference between WT and *eaat5b* mutant fish (two proportions z-test $p>0.05$) (C left). Comparing stimulus intensity-specific responses also leads to a non-significant difference (Kolmogorov-Smirnov test $p>0.05$) (C right). For all graphs in the figure: top shows fish specific results through the whole assay (left) and pooled events distribution over single epoch (right); bottom shows summary statistics as total response proportions (successful hunting responses/ delivered stimuli) and intensity specific percentages (reaction percentage/ stimulus intensity).

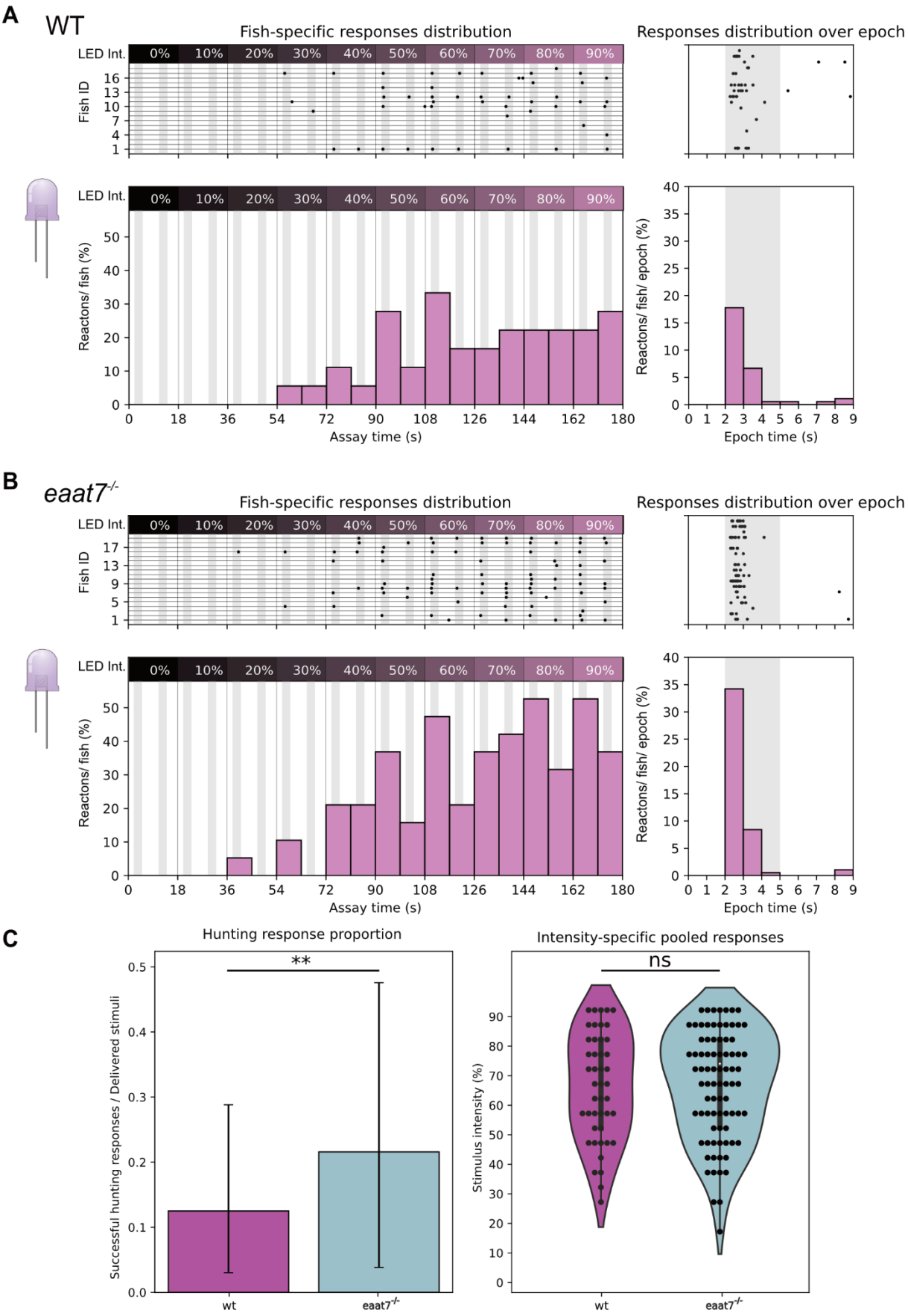


**Figure 6: *eaat7* KO mutants exhibit a higher peak response to an artificial UV prey stimulus compared to WT.**

*eaat7* mutants begin reacting to the incremental prey stimulus one intensity-step later than WT and display overall higher reactions/fish. While WT larvae start showing responses with stimuli delivered at 30% of intensity (A left), *eaat7* mutants start showing reactions from 20% (B left). Both WT and *eaat7* mutant larvae reach peak responses at intensity 90% but surprisingly fish lacking the glutamate transporter show a markedly higher response (A left) compared to WT (B left). Pooled responses proportion is significantly increased in *eaat7* mutant fish compared to WT (two proportions z-test p=0.0011) (C left). Comparing stimulus intensity-specific responses leads to a non-significant difference instead (Kolmogorov-Smirnov test p>0.05) (C right). For all graphs in the figure: top shows fish specific results through the whole assay (left) and pooled events distribution over single epoch (right); bottom shows summary statistics as total response proportions (successful hunting responses/ delivered stimuli) and intensity specific percentages (reaction percentage/ stimulus intensity).

## *eaat5b*$^{-/-}$ but not *eaat7*$^{-/-}$ fish have a lower OMR response to red and black bands

Our monochromatic ERGs showed that lack of either EAAT5b or EAAT7 leads to a lower b-wave generation upon red light stimulation. To confirm this result, we designed a high-throughput OMR assay targeting the zebrafish long-wavelength cones by exposing 5 dpf larvae to moving gratings in black and red in a range of different contrasts delivered in pseudo-random order (Fig. 7A-B). Fish were exposed to two stimuli, one still (habituation phase) and one moving towards the right (stimulus phase), alternated by black and white centering stimuli to reposition the larvae at the center of the arena (Fig. 7B). Next, we calculated each fish rightward movement percentage during both habituation and stimulus phases to observe whether EAATs mutants would perform worse than their WT controls. While during the habituation phase movement direction remains neutral (~50% to either side), all fish displayed a rightward movement increasing along with the delivered black-vs-red contrast during the stimulus phase (Fig. 7C). As expected, *eaat5b* mutants show a marked reduction on the time spent swimming towards the stimulus, particularly at the higher contrasts (contrast: 213; p = 0.01) (Fig. 7C). Interestingly, *eaat7*$^{-/-}$ fish do not show any visible defect when compared with WT even if monochromatic ERG data showed a marked decrease in their b-wave. Both mutants increase overall movement in a contrast-dependent trend with no significant differences from the respective WT control groups (Fig. S2). The optomotor response draws information from both the ON and OFF pathway, and it is conceivable that removing EAAT7 would not generate a defect large enough to be measured by our assay.

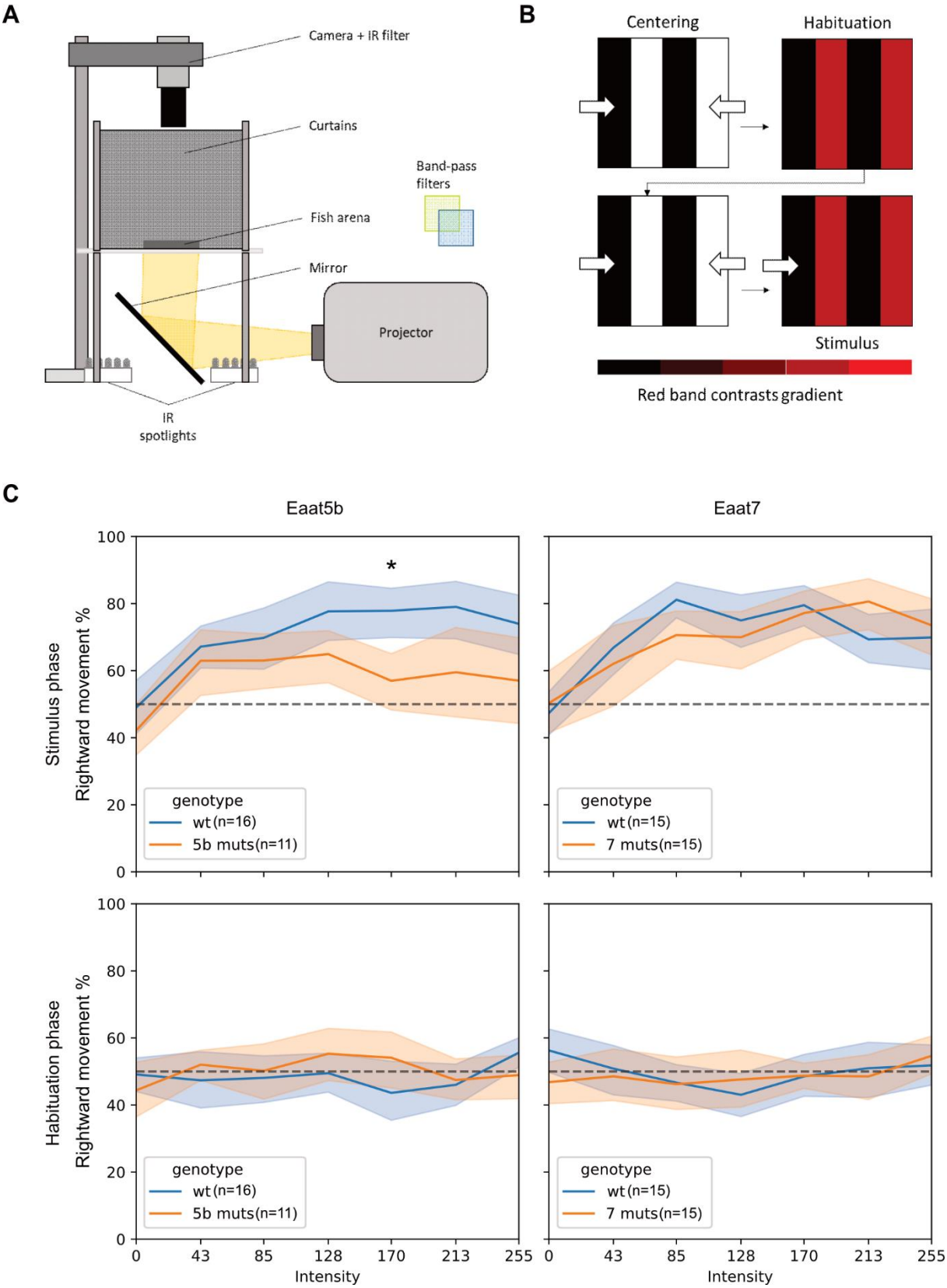


**Figure 7: *eaat5b* but not *eaat7* mutants show lower response to high contrast long wavelength OMR.**
(A) To test long-wavelength range sensitivity, we build an OMR setup where a projector sends moving grating at the bottom of an arena organized in rows. Fish swimming in the rows are tracked by a high-speed camera. (B) We provide a long wavelength targeting paradigm divided in four steps, where two centering stimuli composed by black and white gratings moving towards the center of the arena, guide the larvae in a central position. After

each centering stimulus, still (during the Habituation phase) and rightward-moving (during the Stimulus phase) gratings composed of black and red (at different contrasts) bands are displayed and the larval rightward movement percentage over total movement is calculated for both the long-wavelength phases. (C) The setup was used for testing sensitivity loss in both *eaat* mutants. As expected, *eaat5b* mutants have an overall reduced response to the stimulus (top left), particularly significant at higher contrasts (Repeated measure Anova; $p<0.05$). Conversely, *eaat7* mutants do not show such a defect (top right). In all the tests, fish exposed to a still stimulus (Habituation phase) have no preference independently of the contrast displayed.

## Discussion

In this study, we tested wavelength-specific activity of the postsynaptic EAAT5b and EAAT7 by performing monochromatic ERG assays (Zang et al., 2015). We found that lack of EAAT5b and EAAT7 leads to modest reductions in the ON-response under UV-blue and red light. The lack of measurable defects when the eyes are exposed to green light suggests that these proteins might have a negligible role in conveying light-ON responses received from green cones. UV and blue cones' light sensitivities strongly overlap, making it difficult to isolate cone subtype specific response by recording from the whole-retina with a wide-field stimulus (Yoshimatsu et al., 2021). Hence, effects originating in the UV/blue wavelengths might be buffered by the activity of the unaffected cone population. Since UV cones are crucially involved in prey capture behavior (Yoshimatsu et al., 2020), complementing the ERG analyses with a hunting assay to test UV-light response would potentially reveal masked effects and clarify Eaat5b and Eaat7 wavelength-dependence. By performing whole mount immunohistochemistry staining for EAAT5b, EAAT7, and UV and red cones on 6 dpf dissected retinas, we observed that EAAT5b and EAAT7 are largely co-expressed at most dendritic tips. EAAT7 is uniformly distributed throughout the retina apart from a small region in the SZ, where its relative intensity drops. Conversely, EAAT5b's signal raises in this specific area. By measuring and comparing OPL relative intensity of the UV cone pedicles and the two post-synaptic EAATs, we concluded that UV-prey-detection that the distribution of EAAT5b strongly correlates with these photoreceptors' pattern, particularly in the SZ. Similarly, EAAT7 distribution is concentrated in the nasal patch, where both UV and red cone density is higher. Work investigating the importance of UV cones for prey-capture circuits proposed that while UV-sensitive photoreceptors in the SZ are important for hunting, the morphologically similar cones in the nasal patch might be used to monitor the periphery for predators (Yoshimatsu et al., 2020). Strong relative intensity of EAAT7 in this region, opposed to EAAT5b accumulation by the SZ, might help dealing with the dynamics of these two different visual inputs (paramecia are UV-bright and move with a definite pattern and speed, different from the UV-dark looming shapes of a potential predator). Tracking *eaat7*$^{-/-}$ larvae escape reactions when exposed to a looming stimulus presented in the periphery of their field of view might show if this protein is important or not for this kind of dynamics detection. As expected from the ERG analyses, the relative intensity patterns along the OPL of both EAAT5b and EAAT7 appear to correlate with the red cones pedicles, excluding the SZ where the distribution of these cone-types drops. Previous work from our group showed that in adult retinal sections EAAT5b and EAAT7 appear on dendritic tips contacting all the cone subtypes (Niklaus et al., 2024); we propose that this anisotropy could be present only in contact with UV-cones. Interestingly, preliminary data on mGluR6b distribution in the OPL suggest that this metabotropic receptor follows a distribution pattern close to EAAT5b's, with its signal's relative intensity peaking in the SZ. While expression data on EAATs single mutants did not show any significant difference in mRNA of the functional gene upon KO of either *eaat5b* or *eaat7* (Niklaus et al., 2024), we do

not know whether distribution of EAAT5b would be altered in *eaat7* mutants or vice versa. It is also unknown whether if mGluR6b expression or localization would be somehow perturbed by the absence of one or more EAATs. In the future, it will be worth investigating whether mGluR6b and EAATs constitute a single balanced system or two separate functional units in terms of expression regulation and localization. Another unexplored aspect of this is whether lack of EAAT5B or EAAT7 might change connectivity between specific BC populations and wavelength-specific photoreceptors in the developing retina. Performing BC-tuning assays as previously done by the Baden lab (Bartel et al., 2021) might indicate disruptions in the previously observed tuning patterns. The peculiar localization of EAAT5b in the SZ, along with the observed defect in the UV/Blue range upon KO, suggests an involvement of EAAT5b in prey-detection and capture. Hunting behavior has been extensively studied in the past years, both using live paramecia (Semmelhack et al., 2014; Yoshimatsu et al., 2020) and virtual assays (Bianco et al., 2011; Semmelhack et al., 2014) where generally a moving white dot is projected on a screen and displayed to a larva. In order to test UV-specific sensitivity in our mutants, we built a behavioral setup to deliver UV-bright artificial stimuli simulating swimming paramecia to head-mounted larvae. The setup delivers programmable stimuli at different light intensities and can be used to determine wavelength detection thresholds. We validated the setup testing WT fish reactions to either yellow or UV light, assessing first that UV light responses largely outnumber yellow ones and second that UV response rate is directly proportional to light intensity. When testing our postsynaptic *eaat* mutants, we observed that KO of *eaat5b* does not significantly affect prey-detection and capture behavior. Surprisingly, mutants for EAAT7 showed an increased response rate, and even lower threshold when compared to WT. White light ERG analyses of double KO for these two transporters show that in absence of both the proteins, depolarization dynamics mirror the ones observed upon KO of *eaat5b* alone (Niklaus et al., 2024). In the future, we plan to test whether this would happen when testing double KO with our hunting test. While a previous publication from our group shows that *mglur6b* mutants lose the majority of ON response from ERG experiments (Huang et al., 2012), considering the distribution of both EAAT5B and mGluR6b in the larval retina, testing our new hunting-response assay in mutants lacking this metabotropic receptor might reveal new insights in its role in prey-capture dynamics. These results may be accounted for by the different dynamics of EAAT5b and EAAT7. Namely, removal of EAAT5b leads to a shortening of the time to peak of the measured b-waves, while EAAT7 causes a lengthening of the same, indicating opposing roles in regulating the ON-BCs depolarization timing (Niklaus et al., 2024). UV cones in the SZ have longer signal integration compared to the other photoreceptors, supposedly to better track a moving prey (Yoshimatsu et al., 2020). The concentration of EAAT5b in the BC terminals of this region might be another mechanism to slow down the signal and facilitate this behavior. Loss of EAAT5b might then result in a reduced prey-tracking ability; while conversely, the absence of a functional EAAT7 could lead to slower integration times throughout the whole retina, consequently making stimulus sensitivity higher. To test this, we could modify our existent assay, displaying the moving dot approaching from the periphery of the larval eye and observing if the animal's "detection field" in absence of Eaat7 has expanded outside of the SZ in comparison to mutants. This could be measured by tracking the position of the moving dot once the fish displays prey tracking. Monochromatic ERG revealed long-wavelengths sensitivity defects

in both *eaat5*b and *eaat7* mutants. To confirm these wavelength-specific defects, we built a behavioral setup to present our mutant larvae with OMR-eliciting moving gratings, displaying black and red bands with different contrasts. Our tests showed that while *eaat5b* mutants show a decreased response to the stimulus, no significant difference was observable between WT and *eaat7* mutants. OMR is triggered by both ON- and OFF- stimuli (Orger and Baier, 2005; Kist and Portugues, 2019), and zebrafish larvae tend to respond equally to both of these contrast changes when their field of view is restricted (as in our assay). It is thus possible that effects on the ON-response would be buffered by the fish still strongly responding to light-dark transitions. Behavioral assays can be easily structured to deliver high-throughput results with intuitively measurable effects. However, these results are the outcome of the whole neural circuit, making it difficult to assess complex mechanisms without more targeted assays. Both *eaat5b* and *eaat7* transcripts are expressed throughout the brain (Niklaus et al., 2024), and both localization and effects of their loss in the zebrafish brain are yet to be investigated. Combining monochromatic ERGs with full retinal immunohistochemistry and behavioral experiments finally helped us understand more about the functions and differences of these two postsynaptic transporters. Taken together, our data suggests that while mGluR6b remains the main regulator of ON-BCs depolarization throughout the retina, EAAT5b and EAAT7 modulate response speeds in different regions of the retina to optimize behavior-specific integration dynamics, particularly in relation to UV light. In the future, analysis of published single-cell-transcriptomics databases could help identify whether *eaat5b* and *eaat7* are co-localized in all ON-bipolar cells or if they are, at least in some cases, segregated in different cell populations.

## Material and Methods

### Fish husbandry

Zebrafish (*Danio rerio*) were maintained at a standard 14 h light:10 h dark cycle (LD) with light on at 8 am and light off at 10 pm as previously described (Mullins et al., 1994).Water temperatures were kept between 26 and 28 °C. Fish from the AB and TU wildtype strains were used in our study. Embryos were raised in E3 medium (5 mM NaCl, 0.17 mM KCl, 0.33 mM CaCl2, and 0.33 mM MgSO4) containing 0.01 % methylene blue to suppress fungal growth or in 1-phenyl-2-thiourea (PTU, Sigma-Aldrich) if prevention of pigment formation was required. Embryos were collected directly after laying. Embryos were then transferred to the incubation room with normal light cycle (14:10). Both 5 and 6 days post fertilization (dpf) animals were sacrificed in ice water, following second killing method via freezing at -20°C.The following transgenic lines were used for immunohistochemistry: *Tg(zfSWS1–5.5A:EGFP)* and *Tg(zfLWS:EGFP)* (Tsujimura et al., 2010) expressing EGFP in UV and red cones respectively (Allison et al., 2010). The following mutant lines were used for ERGs and behavioral assays: *eaat5b*$^{-/-}$, *eaat7*$^{-/-}$ and double mutants *eaat5b*$^{-/-}$; *eaat7*$^{-/-}$ (Niklaus et al., 2024).

### Ethics statement

All animal experiments were non-invasive behavioral tests. They were carried out in line with the ARVO Statement for the Use of Animals in Ophthalmic and Vision Research and were approved by the Veterinary Authorities of Kanton Zurich, Switzerland (TV4206).

### Monochromatic electroretinograms

Monochromatic electroretinograms (ERG) of WT and mutant animals were recorded at 5 dpf in a double blinded manner. Larvae were dark adapted for at least 30 min and preparations prior to recordings were performed under a

dim red light to prevent bleaching of photo pigment. The larval eye was removed and placed on filter paper over an agarose gel. The reference electrode was inserted into the agarose gel and the recording electrode, a glass capillary GC100-10 (Harvard Apparatus, Holliston USA) with a tip diameter of 20-30 µm filled with E3 was placed on top of the cornea.
A series of monochromatic light stimuli of 5 different light intensities (log -4 to log 0) were projected to the eyes. Each stimulus was 100 ms with an inter stimulus interval of 7 sec. A high-power xenon light source HPX-2000 (Ocean Optics) was used for monochromatic light stimulation and an additional light source (Philips projection lamp type 6958, 20 V, 250 W in a Liesegang Diafant 250 housing) was used for background adaptations. Different light filters were placed in front of both, stimulation and background light source (see Table 1).

**Table 1**

| Monochromatic stimulation | Stimulation light filter | Background light filter |
|---|---|---|
| UV-Blue light | 350-430 nm (peak at 415 nm) | 500-680 nm |
| Green light | 450-475 nm | >480 nm |
| Red light | >580 nm | none |

## Analysis of ERG data

ERG traces were analyzed using Microsoft Excel and Igor-Pro Software (Wave Metrics). B-wave amplitudes were analyzed as a proxy for ON-bipolar cell depolarization. The first 50 ms of each recording were averaged and taken as baseline values. B-wave amplitudes were statistically compared between WT and mutant animals by multiple two-tailed t tests with multiple comparisons correction using the Holm-Šídák method. All ERG results are plotted in box-and-whisker plots with box showing the quartiles of the respective datasets while the whiskers extend to show the rest of the distribution, except for points that are determined to be “outliers” (outside of interquartile range * 1.5) as of default with the “seaborn” Python library boxplots. The boxplots are overlaid with a swarm plot representing single fish amplitudes.

## Immunohistochemistry

6 dpf larvae were raised in 0.0003 g/ml phenylthiourea (PTU), sacrificed by incubation in ice water (0°C) and fixed with 1% trichloroacetic acid (TCA) and 2% Sucrose (in PBS) for 60 min at room temperature (RT). After washing in PBS, eyes were dissected and permeabilized by rinsing with proteinase K solution (0.02 mg*ml in PBS).
Dissected eyes were post-fixed in 1% TCA, 2% Sucrose in PBS solution for 20 min, washed in PBT (Triton-X100 0.8% in PBS) and blocked in blocking solution (10% normal goat serum, 1% bovine serum albumin in PBT) for one hour. Primary antibodies diluted in blocking solution were applied overnight (ON) at 4°C. The following antibodies were used: guinea pig anti-Eaat5b (1:100), rabbit anti-Eaat7 (1:400), chicken anti-GFP (A20162; Invitrogen) (1:500). Primary antibodies were detected with the following secondary antibodies (all 1:500 in PBS) for ON at 4°C: goat anti-rabbit, goat anti-guinea pig, goat anti-chicken and goat anti-mouse all conjugated to Alexa Fluor (AF) 488, 568 or 647 (Invitrogen, Molecular Probes). Cells nuclei were stained with 4’,6-diamidino-2-phenylindole (DAPI) (1:1000 in PBS). Eyes were embedded in Mowiol-DABCO and confocal laser scanning imaging was performed with a TCS LSI confocal microscope (Leica). Full retina stacks were recorded with a 40x oil-immersion

micro-objective scanning the whole OPL surface in 1 µm steps.

### Image processing and data analysis

Full retina stacks were opened in the software Fiji (ImageJ) (Schindelin et al., 2012) and a virtual mid-section, defined as the section in which the three nuclear layers lay perpendicular to the image plane, was selected. Using morphological landmarks in the photoreceptor (UV or Red cones) channel, a segment line was traced along the whole OPL starting from the ventral side of the Strike Zone. The ROI thickness lying under the set line was then enlarged to 20px and the signal intensity laying under the whole ROI was recorded for every channel.

OPL intensities were analyzed through a Python script: traces were imported as Data frame, the photoreceptor, Eaat5b and Eaat7 channel intensities were normalized over DAPI and divided by trace-specific maximum value. This led to obtain relative intensities with values spanning from 0 to 1. Intensity reading lengths were also normalized to fit between 0 and 1, making each eye comparable with the other. Relative intensities were then smoothened using a rolling average with a window of 25points (over an average of 3000 data points per trace). Single traces were inserted in a correlation matrix and statistically tested with Pearson's correlation to observe Eaat5b and Eaat7 distribution similarities with both UV and Red cones pedicles.

### Hunting assays

All hunting assays were performed with a custom-built setup composed by a 3.5cm platform hosting 2 pairs of infra-red (800-920nm; OSRAM) LEDs and one white LED (420-650nm; Elegoo) for tracking camera/background lightning respectively. An overhead high-speed camera (Pike F032B ASG16; Allied Vision) with a 12mm objective was fixed on an adjustable holder and centered over the platform. At 2 cm from the platform, a custom optics adapter holding a double convex lens (focal length = 22.65 mm; Edmund Optics), a 0.5mm pinhole wheel, a plano-convex lens (focal length = 10 mm; Spindler&Hoyer) and a 5mm LED (orange: 550-620 nm; Sander/ ultraviolet: 340-380nm; Roithner LaserTechnik) was fixed on top of a servomotor (SG90; Tower Pro). Both servomotor and LED were connected to a microcontroller (Arduino UNO; Elegoo) for stimulus control of intensity and movement. Camera and microcontroller were both operated by Stytra (Štih et al., 2019), a Python-based open-source behavioral software able to track several behaviors and administer a series of programmed stimuli. 6 dpf larvae were mounted on an arena built from a 3.5cm Petri dish cap. The forward half of the rim was removed to prevent excessive UV absorption and light refraction from the plastic. A screen made from laminated printing paper was glued to it. Larvae were mounted in 2% low melting agarose (Sigma-Aldrich) and positioned in the center of the arena at ~7 mm from the screen. Once the agarose was set, the arena was filled with E3 medium and a scalpel was used to free both tail and head, making sure that the larva could move its eyes. The used tracking protocol measured eye-specific angle over time coupled with tail curvature. Both parameters were collected from the analysis but tail tracking was not considered during data processing due to the very noisy traces given by the system's lightning conditions.

### Maximum intensity hunting assay

Larvae were exposed to a series of 20 stimuli proceeding in alternate directions. After 2 s of standby, the LED turns on, projecting a ~4.9° stimulus in front of the larva. The projected dot moves towards either left or right at ~33°/s, ending after 3 s at ~90° of the larval field of view, due to the properties of the arena. When

the stimulus stops moving, it turns off the LED and resets its position. Stimuli alternate in direction and always start with a left-right movement in the larva perspective. All stimuli are delivered with LED intensity at 100%.

### Incremental intensity hunting assay

The assay is structured as described under the "Maximum intensity hunting assay" section. Here, light intensity is delivered in 10 steps of intensity, with each step replicated for each stimulus direction (left-right, right-left). The intensity steps go from 0% (used as a no-stimulus control), up to 90%. We stopped at this level after observing a performance drop directly after intensity at 70% (probably due to stimulus habituation).

### Hunting assays data analysis

Raw tracking data obtained by Stytra (Štih et al., 2019) was analyzed in Python. The designed event-detection algorithm compares the raw eye angle tracks with a rolling average of the same trace to detect peaks and compare their amplitude with a set threshold based on the average noise of the trace itself. If both eyes have a convergence (inward turn of the eye) event (prey locking) or if one single eye strongly converges (prey tracking) an event is registered. The same procedures apply for the tail by comparing raw total tail curvature to a rolling averaged trace, assigning an event when the curvature peaks in the direction of the stimulus movement (tail recordings have not been used due to tracking difficulties). A second script pools information from all the fish and plots fish-specific single events along with total event frequency per epoch or for each delivered stimulus. Total responses over delivered stimuli are tested for significance via two proportions z test (CI measured via Wilson method), while intensity-specific response distributions are tested via Kolmogorov-Smirnov test.

### Long-wavelength specific OMR assay

OMR assays were performed on a custom-built setup composed by: a 3d printed arena (11 rows 1x16cm) glued on clear glass and positioned on a diffuser panel, a projector (hp vp6111) to display moving gratings controlled by the Python-based software Stytra (Štih et al., 2019) and a high-speed camera (Stingray F046B ASG, Allied Vision) mounting an IR filter on a 12.5mm objective (FUJINON CF12.5HA-1). A bottom IR light source (infrared spotlight baustein, Kemo Electronics) provides the illumination for the camera feed. The stimulation paradigm was divided into four stages: a centering stimulus with black and white gratings moving towards the center of the arena, a still red and black grating to observe basal movement direction preference, a second centering stimulus and finally a rightward moving grating stimulus. Zebrafish larvae were exposed to seven different red contrasts in a pseudo-random order. Specifics of the stimuli are showed in Table 2. Raw tracking data (fish coordinates over time) was analyzed in Python. The recorded area from the camera was divided into 10 ROIs that included the 10 rows with larvae in it. Coordinates inside each ROI were assigned to the respective fish. Zebrafish larvae travelled distance was measured by calculating the distance between consecutive coordinates and summing them. Movement towards the stimulus direction (rightward) was measured by filtering through consecutive coordinates for which the x values were increasing. Speed between each coordinate was calculated and filtered for movements over double their average speed (~29mm/s) (Danielle Clift et al., 2014). Data from multiple assays was pooled and rightward movement during both habituation (still colored grating) and stimulus phase (rightward-moving colored grating) were compared. Statistical significance was calculated by repeated measures Anova with the software GraphPad Prism 9.5.0.

**Table 2**

| | |
|---|---|
| **Red band contrasts** | 170 – 43 – 255 – 85 – 0 – 213 – 128 |
| **Red gratings wavelength range** | >550 nm; peak at 596 nm |
| **Gratings speed** | Centering/ Rightward: 14.5 mm/s<br>Habituation: 0 mm/s |
| **Gratings period** | 6 mm |
| **Paradigm structure** | Centering stimulus (30s) – habituation (30s) – centering stimulus (30s) – rightward stimulus (30s) |
| **Camera exposure** | 30 ms |


## Acknowledgements

All authors would like to thank Martin Walther, Kara Kristiansen and Heidi Mockel for excellent technical assistance and animal care taking. We also would like to thank Prof. Dr. Tom Baden and Prof. Dr. Martin Müller for excellent suggestions and insights throughout the whole project. This work was funded by the Swiss National Science Foundation (310030_204648 and 310030_200376).


## References


Allison, W. T., Barthel, L. K., Skebo, K. M., Takechi, M., Kawamura, S., and Raymond, P. A. (2010). Ontogeny of cone photoreceptor mosaics in zebrafish. *J Comp Neurol* 518, 4182–4195. doi: 10.1002/cne.22447

Bartel, P., Yoshimatsu, T., Janiak, F. K., and Baden, T. (2021). Spectral inference reveals principal cone-integration rules of the zebrafish inner retina. *Current Biology* 31, 5214-5226.e4. doi: 10.1016/j.cub.2021.09.047

Bianco, I. H., Kampff, A. R., and Engert, F. (2011). Prey capture behavior evoked by simple visual stimuli in larval zebrafish. *Front Syst Neurosci* 5, 101. doi: 10.3389/fnsys.2011.00101

Danielle Clift, Holly Richendrfer, Robert J. Thorn, Ruth M. Colwill, and Robbert Creton (2014). High-Throughput Analysis of Behavior in Zebrafish Larvae: Effects of Feeding. *Zebrafish* 11, 455. doi: 10.1089/zeb.2014.0989

Euler, T., Haverkamp, S., Schubert, T., and Baden, T. (2014). Retinal bipolar cells: elementary building blocks of vision. *Nat Rev Neurosci* 15, 507–519. doi: 10.1038/nrn3783

Fahlke, C., Kortzak, D., and Machtens, J.-P. (2016). Molecular physiology of EAAT anion channels. *Pflugers Arch* 468, 491–502. doi: 10.1007/s00424-015-1768-3

Fairman, W. A., Vandenberg, R. J., Arriza, J. L., Kavanaugh, M. P., and Amara, S. G. (1995). An excitatory amino-acid transporter with properties of a ligand-gated chloride channel. *Nature* 375, 599–603. doi: 10.1038/375599a0

Gesemann, M., Maurer, C. M., and Neuhauss, S. C. F. (2010). Excitatory amino acid transporters in the zebrafish: Letter to "Expression and functional analysis of Na(+)-dependent glutamate transporters from zebrafish brain" from Rico et al. *Brain Res Bull* 83, 202–206. doi: 10.1016/j.brainresbull.2010.04.018

Huang, Y.-Y., Haug, M. F., Gesemann, M., and Neuhauss, S. C. F. (2012). Novel expression patterns of metabotropic glutamate receptor 6 in the zebrafish nervous system. *PLoS One* 7, e35256. doi: 10.1371/journal.pone.0035256

Kist, A. M., and Portugues, R. (2019). Optomotor Swimming in Larval Zebrafish Is Driven by Global Whole-Field Visual Motion and Local Light-Dark Transitions. *Cell Rep* 29, 659-670.e3. doi: 10.1016/j.celrep.2019.09.024

Mim, C., Balani, P., Rauen, T., and Grewer, C. (2005). The glutamate transporter subtypes EAAT4 and EAATs 1-3 transport glutamate with dramatically different kinetics and voltage dependence but share a common uptake mechanism. *J Gen Physiol* 126, 571–589. doi: 10.1085/jgp.200509365

Morgans, C. W., Brown, R. L., and Duvoisin, R. M. (2010). TRPM1: the endpoint of the mGluR6 signal transduction cascade in retinal ON-bipolar cells. *Bioessays* 32, 609–614. doi: 10.1002/bies.200900198

Morgans, C. W., Zhang, J., Jeffrey, B. G., Nelson, S. M., Burke, N. S., Duvoisin, R. M., et al. (2009). TRPM1 is required for the depolarizing light response in retinal ON-bipolar cells. *Proc Natl Acad Sci U S A* 106, 19174–19178. doi: 10.1073/pnas.0908711106

Mullins, M. C., Hammerschmidt, M., Haffter, P., and Nüsslein-Volhard, C. (1994). Large-scale mutagenesis in the zebrafish: in search of genes controlling development in a vertebrate. *Curr Biol* 4. doi: 10.1016/s0960-9822(00)00048-8

Nelson, R. F., and Singla, N. (2009). A spectral model for signal elements isolated from zebrafish photopic electroretinogram. *Vis Neurosci* 26, 349–363. doi: 10.1017/S0952523809990113

Niklaus, S., Cadetti, L., Vom Berg-Maurer, C. M., Lehnherr, A., Hotz, A. L., Forster, I. C., et al. (2017). Shaping of Signal Transmission at the Photoreceptor Synapse by EAAT2 Glutamate Transporters. *eNeuro* 4. doi: 10.1523/ENEURO.0339-16.2017

Niklaus, S., Glasauer, S. M.K., Kovermann, P., Farshori, K. F., Cadetti, L., Früh, S., et al. (2024). Glutamate transporters are involved in direct inhibitory synaptic transmission in the vertebrate retina. *Open Biol* 14. doi: 10.1098/rsob.240140

Orger, M. B., and Baier, H. (2005). Channeling of red and green cone inputs to the zebrafish optomotor response. *Vis Neurosci* 22, 275–281. doi: 10.1017/S0952523805223039

Saszik, S., Alexander, A., Lawrence, T., and Bilotta, J. (2002). APB differentially affects the cone contributions to the zebrafish ERG. *Vis Neurosci* 19, 521–529. doi: 10.1017/s0952523802194144

Schindelin, J., Arganda-Carreras, I., Frise, E., Kaynig, V., Longair, M., Pietzsch, T., et al. (2012). Fiji: an open-source platform for biological-image analysis. *Nat Methods* 9, 676–682. doi: 10.1038/nmeth.2019

Semmelhack, J. L., Donovan, J. C., Thiele, T. R., Kuehn, E., Laurell, E., and Baier, H. (2014). A dedicated visual pathway for prey detection in larval zebrafish. *Elife* 3. doi: 10.7554/eLife.04878

Spence, R., Gerlach, G., Lawrence, C., and Smith, C. (2008). The behaviour and ecology of the zebrafish, Danio rerio. *Biol Rev Camb Philos Soc* 83, 13–34. doi: 10.1111/j.1469-185X.2007.00030.x

Štih, V., Petrucco, L., Kist, A. M., and Portugues, R. (2019). Stytra: An open-source, integrated system for stimulation, tracking and closed-loop behavioral experiments. *PLoS Comput Biol* 15, e1006699. doi: 10.1371/journal.pcbi.1006699

Tsujimura, T., Hosoya, T., and Kawamura, S. (2010). A single enhancer regulating the differential expression of duplicated red-sensitive opsin genes in zebrafish. *PLoS Genet* 6, e1001245. doi: 10.1371/journal.pgen.1001245

Wang, X., Roberts, P. A., Yoshimatsu, T., Lagnado, L., and Baden, T. (2023). Amacrine cells differentially balance zebrafish color circuits in the central and peripheral retina. *Cell Rep* 42, 112055. doi: 10.1016/j.celrep.2023.112055

Wong, K. Y., and Dowling, J. E. (2005). Retinal bipolar cell input mechanisms in giant danio. III. ON-OFF bipolar cells and their color-opponent mechanisms. *J Neurophysiol* 94, 265–272. doi: 10.1152/jn.00271.2004

Yoshimatsu, T., Bartel, P., Schröder, C., Janiak, F. K., St-Pierre, F., Berens, P., et al. (2021). Ancestral circuits for vertebrate color vision emerge at the first retinal synapse. *Sci Adv* 7, eabj6815. doi: 10.1126/sciadv.abj6815

Yoshimatsu, T., Schröder, C., Nevala, N. E., Berens, P., and Baden, T. (2020). Fovea-like Photoreceptor Specializations Underlie Single UV Cone Driven Prey-Capture Behavior in Zebrafish. *Neuron* 107, 320-337.e6. doi: 10.1016/j.neuron.2020.04.021

Zang, J., Keim, J., Kastenhuber, E., Gesemann, M., and Neuhauss, S. C. F. (2015). Recoverin depletion accelerates cone photoresponse recovery. *Open Biol* 5. doi: 10.1098/rsob.150086

Zimmermann, M. J.Y., Nevala, N. E., Yoshimatsu, T., Osorio, D., Nilsson, D.-E., Berens, P., et al. (2018). Zebrafish Differentially Process Color across Visual Space to Match Natural Scenes. *Current Biology* 28, 2018-2032.e5. doi: 10.1016/j.cub.2018.04.075

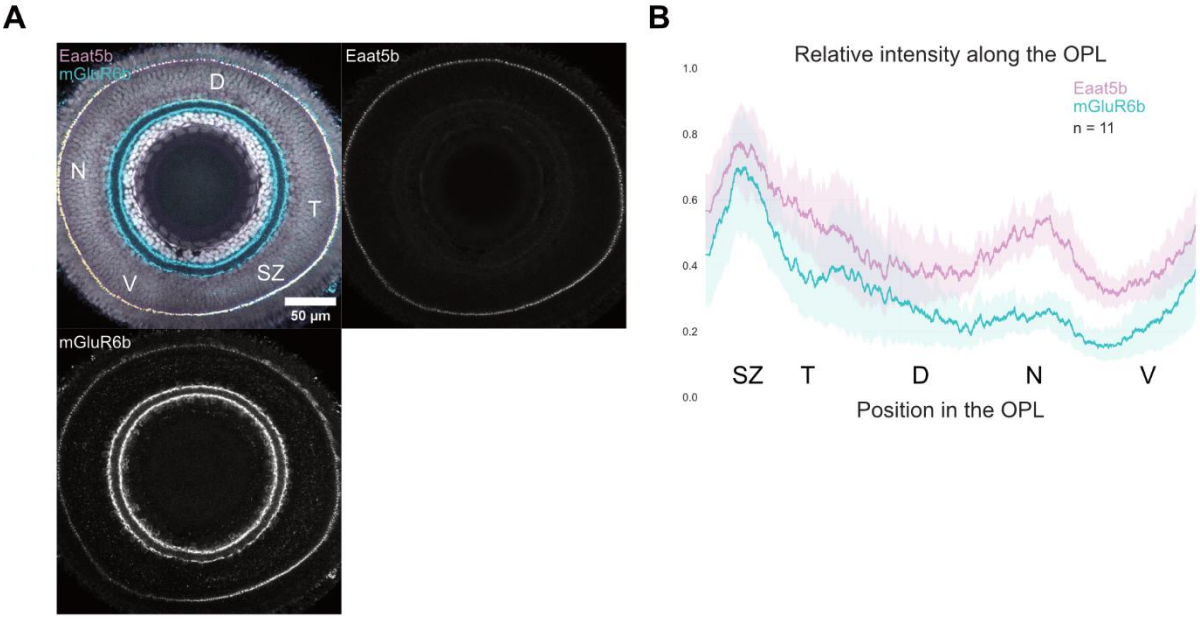


**Figure S1: mGluR6b OPL distribution peaks in the SZ in a similar pattern to Eaat5b.**
(A) Virtual midsection of a 6 dpf WT retina with nuclei (grey), mGluR6b (cyan) and EAAT5b (magenta) labelled. (B) Relative intensity values of the two fluorescent channels along the whole OPL. Full-colored line represents the traces' mean and semitransparent area represents 95% CI.

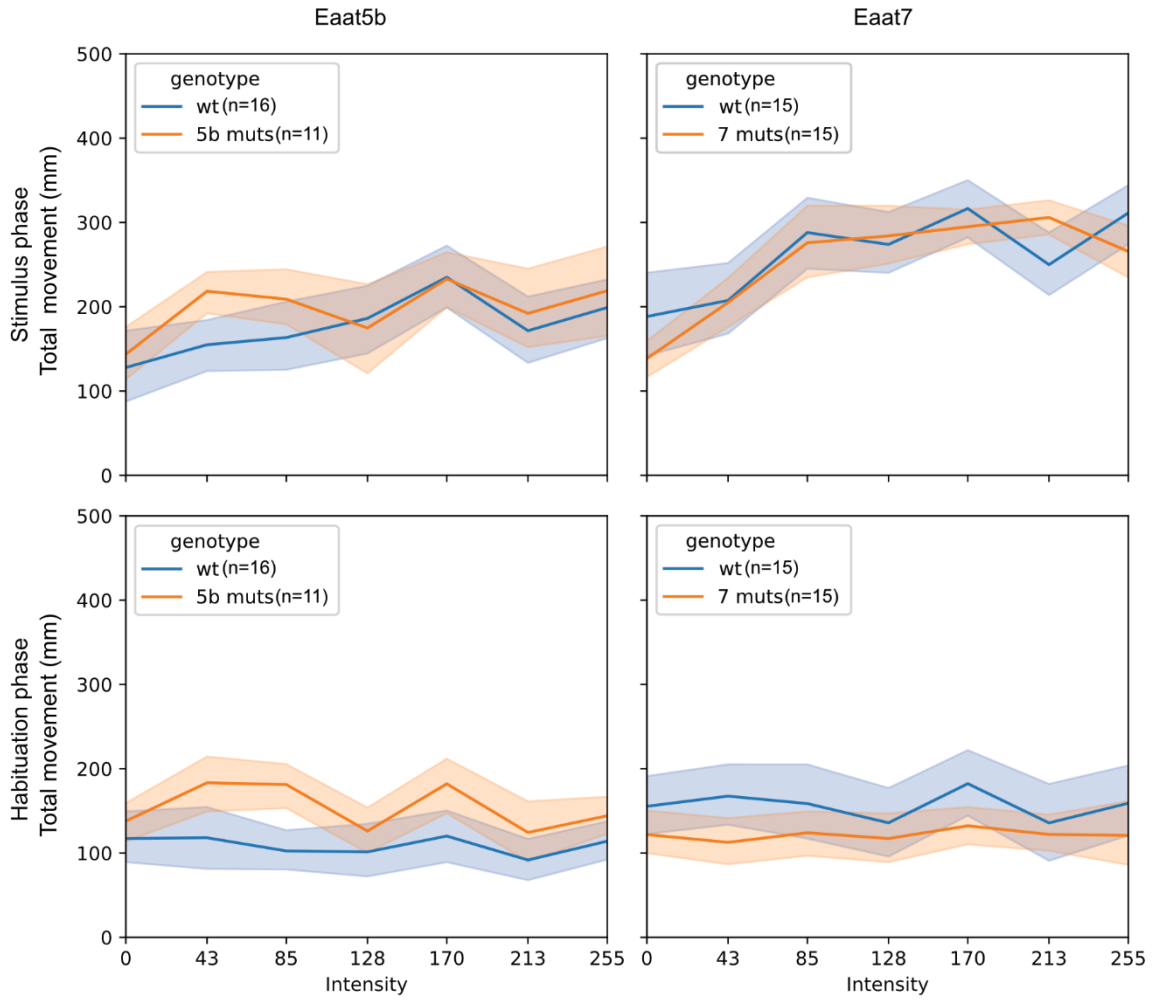


**Figure S2: *eaat5b* and *eaat7* mutants show same total activity as their respective control groups during black and red OMR assay.**

Average total movement of *eaat*s mutant larvae and their respective control groups exposed to red and black moving gratings at different contrasts. Overall, no major differences in activity can be detected in any of the groups. Both controls and *eaat* mutants show an increase in overall activity while the gratings are moving (top), while activity remains relatively stable when the stimulus remains still (bottom).